



Multiparametric MRI in Diagnosis of Parotid Gland Tumor: An Observational Study in 3-T MRI

Sreecharan V.R.¹ Suprava Naik¹ Nerbadyswari Deep¹ Amit Kumar Adhya² Preetam Chappity³
Sudipta Mohakud¹ Manoj Kumar Nayak¹ Ranjan Kumar Patel¹ Taraprasad Tripathy¹

¹Department of Radiodiagnosis, All India Institute of Medical Sciences, Bhubaneswar, Odisha, India

²Department of Pathology, All India Institute of Medical Sciences, Bhubaneswar, Odisha, India

³Department of ENT, All India Institute of Medical Sciences, Bhubaneswar, Odisha, India

Address for correspondence Dr. Suprava Naik, MD Radiodiagnosis, Department of Radiodiagnosis, All India Institute of Medical Sciences, Bhubaneswar 751019, Odisha, India (e-mail: drsuprava.rd@gmail.com).

Indian J Radiol Imaging

Abstract

Background Preoperative magnetic resonance imaging (MRI) has an important role in the management and prognostication of parotid gland tumors. We aim to evaluate the role of multiparametric MRI in differentiating the major subgroup of parotid tumors.

Material and Methods Multiparametric MRI: T1-weighted imaging (T1WI), T2WI, diffusion-weighted imaging (DWI), pseudo-continuous arterial spin labeling (ASL) and dynamic contrast-enhanced (DCE) imaging were acquired in all patients. Apparent diffusion coefficient (ADC) values and tumor blood flow (TBF) were calculated from DWI and ASL, respectively. Ktrans, Kep, Ve, initial area under the gadolinium enhancement concentration curve (IAUGC), maximum slope, and contrast enhancement ratio (CER) were calculated from DCE-MRI perfusion. The above parameters were compared between three major subgroups of parotid gland tumors, such as non-Warthin benign tumors (NWBT), Warthin's tumors (WT), and malignant parotid tumors (MT).

Results The mean ADC of MT ($n=13$), WT ($n=5$), and NWBT ($n=29$) was $1.03 \times 10^{-3} \text{ mm}^2/\text{s}$, $0.97 \times 10^{-3} \text{ mm}^2/\text{s}$, and $1.89 \times 10^{-3} \text{ mm}^2/\text{s}$, respectively. The mean TBF (in mL/100 g/min) was the highest MT (70.33), followed by WT (62.04) and NWBT (21.99). A cutoff of 40.51 mL/100 g/min showed a sensitivity of 96.6% and specificity of 77.8% for predicting NWBT. In DCE-MRI, 96.6% of the NWBT showed a type A time–signal intensity curve. Although the majority of MT and WT had type C and B curves, respectively, there was overlapping. Among the quantitative DCE parameters, Ktrans and Kep were highly sensitive for differentiating NWBT, WT, and MT. Ktrans, Kep, IAUGC, and MS were maximum in WT, followed by MT and NWBT. Kep and Ktrans both had an accuracy of 84.7% for predicting pleomorphic adenoma.

Conclusion Multiparametric MRI is useful for differentiating NWBT, WT, and MT. DCE-MRI helps in differentiating benign from malignant tumors. DWI and ASL are useful in differentiating NWBT from parotid malignancy.

Keywords

- ▶ diffusion-weighted MRI
- ▶ arterial spin labeling
- ▶ dynamic contrast enhanced MRI
- ▶ parotid tumor
- ▶ salivary gland tumor

DOI <https://doi.org/10.1055/s-0044-1800861>.
ISSN 0971-3026.

© 2024. Indian Radiological Association. All rights reserved.
This is an open access article published by Thieme under the terms of the Creative Commons Attribution-NonDerivative-NonCommercial-License, permitting copying and reproduction so long as the original work is given appropriate credit. Contents may not be used for commercial purposes, or adapted, remixed, transformed or built upon. (<https://creativecommons.org/licenses/by-nc-nd/4.0/>)
Thieme Medical and Scientific Publishers Pvt. Ltd., A-12, 2nd Floor, Sector 2, Noida-201301 UP, India

Introduction

Salivary gland tumors accounts for 2.0 to 6.5% of all head and neck tumors, and approximately 80% of them are localized in the parotid gland.¹ Ultrasonography is used as the initial screening modality, but it has limitations in the visualization of the deep lobe of the parotid gland. Magnetic resonance imaging (MRI) is considered the imaging modality of choice in patients with parotid gland tumors. It is important to characterize the lesion preoperatively for planning surgical and postsurgical management as well as for prognostication. Only superficial parotidectomy is done in benign tumors located in the superficial parotid gland, whereas complete parotidectomy with node dissection with or without radiotherapy is needed in malignant lesions. The sensitivity of preoperative fine needle aspiration cytology (FNAC) in differentiating benign and malignant parotid tumors is variable in different studies (52–98.5%).^{2,3} MRI plays an important role in preoperative workup. Structural sequences of MRI show the signal characteristics and extent of the lesion. Multiparametric MRI with the incorporation of diffusion-weighted imaging (DWI) and dynamic contrast-enhanced MRI (DCE-MRI) provides information regarding the cellularity and contrast kinetics of the lesion. The aim of this study is to assess the accuracy of multiparametric MRI including conventional MRI, DWI, and DCE-MRI in characterizing various parotid gland tumors and in differentiating benign and malignant tumors (MTs) of the parotid gland based on their structural and functional characteristics.

Material and Methods

This was a cross-sectional observational study to assess the accuracy of multiparametric MRI in differentiating benign and MTs in the parotid gland in a tertiary care institute after ethical approval.

Inclusion and Exclusion Criteria

Patients of parotid gland tumor referred for MRI were included in the study after obtaining written informed consent. Patients of all age groups were included in the study. Patients having MRI-incompatible implant or contra-indication for gadolinium contrast agent were excluded.

Sample Size

A total of 47 cases of parotid gland tumors referred for MRI were included in this study.

MRI Protocol

MRI of the parotid gland was performed in all the patients in a 3-T MRI scanner (Discovery 750W, GE Healthcare) using a 48-channel head coil. A standardized imaging protocol was followed in all the patients using the following parameters: axial T1-weighted imaging (T1WI): repetition time [TR]/echo time [TE], 561/9.7 milliseconds; field of view (FOV), 22 × 20 cm; NEX, 2.00; slice thickness, 4 mm; and matrix size, 300 × 300 mm²; axial T2 PROPELLER: TR/TE, 5,757/85.0 milliseconds; FOV, 21 × 20 cm; NEX, 2.00; slice thickness,

4 mm; and matrix size, 448 × 448 mm²; and short tau inversion recovery (STIR): TR/TE, 8,500/53.2 milliseconds; FOV, 24 × 22 cm; NEX, 2.00; slice thickness, 4.0 mm; and matrix size, 320 × 256 mm² in axial and coronal plane; axial DWI: TR/TE, 5,500/67.4 milliseconds; FOV, 24 × 24 cm; NEX, 4.00; slice thickness, 4 mm; and *b*-values, 0 and 1,000. The following pseudo-continuous arterial spin labeling (ASL) parameters were acquired in the axial plane: TR/TE, 4,853/10.7; FOV, 33.7 × 26 cm; NEX, 1.00; and slice thickness, 4.0 mm. Axial DCE-MRI was acquired before, during, and after intravenous (IV) administration of gadolinium contrast agent with the following parameters: TR/TE: 4.8/2.2 milliseconds; frequency FOV: 48.0 cm; NEX: 0.73; slice thickness: 3.0 mm; and matrix size: 320 × 256 mm². Thirty-two phases were acquired at 11-second intervals, contrast was injected after the third phase, and the acquisition time was 5 minutes and 52 seconds. Coronal postcontrast fat saturated (FS) T1WI (TR/TE: 719/8.2 milliseconds; FOV: 24 × 22 cm; NEX: 3.00; slice thickness: 4.0 mm) and postcontrast TIWI FS three-dimensional (3D) sequence (TR/TE: 5. 1/1.7 milliseconds; FOV: 40; NEX: 1.41; slice thickness: 2.0 mm) were also obtained.

Image Analysis

Image analysis was done in the Advantage Workstation provided by GE Medical system. Two experienced radiologists with 15 and 30 years of experience, blinded to the histopathology findings, analyzed all the data independently. Any difference in opinion was resolved by consensus.

The morphological characteristics such as location of the tumor, shape, margin, signal intensity, homogeneity, cystic changes, and infiltration into adjacent structures were assessed on T1WI, T2WI, and postcontrast T1WI, and compared between benign and malignant groups.

DWI was analyzed qualitatively to look for diffusion restriction within the lesion. The apparent diffusion coefficient (ADC) map was derived from the acquired DWI and the ADC value was taken after the placement of the region of interest (ROI) over the lesion. Three ROIs (15–30 mm² in size) were drawn in the solid components of the lesion and the average ADC value was calculated. In solid cystic lesions, the ROI was drawn carefully to include only the solid component of the lesion.

After postprocessing ASL, tumor blood flow (TBF) values were obtained by placing the ROI over the solid component of the lesion. The enhancement pattern was evaluated in post-contrast T1WI. The type of time–signal intensity curve (TIC) was assessed in the GenIQ software of AWS, and categorized into four groups based on the washout ratio (WR) and time to peak (Tpeak): type A = Tpeak > 120 seconds; type B = Tpeak ≤ 120 seconds and WR ≥ 30%; type C = Tpeak ≤ 120 seconds and WR < 30%; and type D = flat TIC.^{4,5}

Quantitative parameters such as transfer factor (Ktrans), fraction of extravascular extracellular space (EES) to the total tumor volume (Ve), flux constant (Kep), initial area under the gadolinium enhancement concentration curve (IAUGC), contrast enhancement ratio (CER), and maximum slope (MS) were derived from the DCE perfusion imaging and values were obtained for all the lesions.

All the cases were categorized into three major subgroups, namely non-Warthin benign tumors (NWBt), Warthin's tumor (WT), and MTs as they have different management and prognosis. The above-mentioned parameters were compared between these groups. All patients underwent surgical biopsy after MRI. Histopathological diagnoses were compared with the MRI diagnosis.

Data Collection and Statistical Analysis

The acquired MRI data were collected and analyzed using the "SPSS software" version 26. The categorical data were presented as the percentage of the total, while the quantitative data were presented as mean and standard deviation. A comparison of the means was done by independent t-test/analysis of variance for parametric data and chi-squared test/Kruskal-Wallis test for nonparametric data. For all the statistical tests used, the level of significance was set at a p-value ≤ 0.05.

Results

A total of 47 patients were included in this study. Twenty-five (53.2%) were males. The mean age of the patients was 45.1 ± 14.92 years ranging from 15 to 72 years. The mean duration of symptoms was 9.1 months in the entire sample. Forty-four patients presented with facial swelling, whereas three patients had complaints of oral cavity swelling. One patient had associated pain. All the cases were unilateral.

Out of 47 cases, 29 (61.7%) were NWBTs, 5 (10.6%) were WTs, and 13 (27.6%) were MTs. Among the NWBTs (n = 29), most of the cases were pleomorphic adenoma (n = 26), two were myoepithelioma, and one case was ancient schwannoma of the intraparotid facial nerve.

Imaging Findings

Morphological Characters

All the round to oval lesions with a well-defined margin were benign. Lesions with well-defined lobulated margins were also favoring benign tumors. Cystic changes were present in 28 cases, out of which 21 were benign. The presence of cystic change had a significant association with benign tumors (p = 0.008).

Four (8.5%) cases showed infiltration into adjacent structures, all of which turned out to be malignant. Two of them had a perineural spread. The details of the clinical presentation and structural MRI findings are presented in ►Tables 1 and 2.

Diffusion-Weighted MRI

The mean ADC values of NWBTs, WTs, and MTs were 1.89 ± 0.43 × 10⁻³ mm²/s, 0.97 ± 0.45 × 10⁻³ mm²/s, and 1.03 ± 0.31 × 10⁻³ mm²/s, respectively. There was a significant difference between the mean ADC of NWBTs and WTs (p = 0.001) and that of NWBTs and MTs (p = 0.001). No significant difference was noted between the mean ADC of WTs and MTs (p = 0.96). A cutoff ADC of 1.35 × 10⁻³ mm²/s showed a sensitivity, specificity, positive predictive value (PPV), negative predictive value (NPV), and accuracy of 93.1, 88.9, 93.1, 88.8, and 91.4%, respectively, for diagnosis of NWBTs with an area under the curve of 0.941 (►Fig. 1A).

Arterial Spin Labeling

The mean TBF of NWBT was 21.99 ± 12.62 mL/100 g/min, which was significantly lower than those of WT (62.04 ± 37.72 mL/100 g/min; p = 0.015) and MT (70.33 ± 36.18 mL/100 g/min; p = 0.001). There was no significant difference in the TBF between WT and parotid malignancy (p = 0.77). Using the ROC curve analysis, a cutoff of 40.51 mL/100 g/min showed a sensitivity of 96.6%, specificity of 77.8%, PPV of 87.5%, NPV of 93.3%, and accuracy of 91.4% for predicting NWBT with an area under the curve of 0.88 (►Fig. 1B).

Dynamic Contrast-Enhanced MRI

Twenty-eight out of 29 (96.6%) NWBT showed type A TIC, 9 out of 13 MTs showed a type C curve, and 3 out of 5 WTs showed a type B curve. One completely cystic WT showed a type D curve. The type A curve had a sensitivity of 96.5%, specificity of 88.8%, PPV of 93.3%, NPV of 94.1%, and an accuracy of 93.6% for differentiating NWBT from other parotid tumors. Type C curve had a sensitivity of 69.2%, specificity of 94.1%, PPV of 81.8%, NPV of 88.8%, and an accuracy of 87.2% for differentiating MTs from other parotid tumors.

There was a statistically significant association between the type of time-intensity curve and the tumor category (p < 0.001).

Table 1 Clinical and demographic parameters of patients with parotid tumor

Parameters	All patients included in the study (n = 47)	Patients with benign parotid tumor (n = 34)	Patients with malignant parotid tumor (n = 13)	p-value
Age (y), mean ± SD (range)	45.1 ± 14.92 (15–72)	41.7 ± 13.67 (15–72)	53.8 ± 14.99 (26–72)	
Duration of symptoms (mo), mean ± SD (range)	9.1 ± 2.9 (4–18)	9.56 ± 3.1 (4–18)	7.92 ± 2.2 (4–12)	0.09
Gender (male/female)	25/22	15/19	10/3	
Unilateral	47/47 (100%)	34/34 (100%)	13/13 (100%)	
Clinical presentation				
Pain	1/47	0/34	1/13	
Swelling	47/47	34/34	13/13	

Table 2 MRI findings of benign and malignant parotid tumors

Parameters	Benign parotid tumor (n = 34)	Malignant parotid tumor (n = 13)	p-value
Unilateral/bilateral	34/0	13/0	
Solitary/multifocal	33/1	11/2	
Shape			
Round or oval	4 (11.8%)	0 (0%)	0.001
Lobulated	23 (67.6%)	3 (23.1%)	0.467
Irregular	7 (20.6%)	10 (76.9%)	
Margin			
Well defined	34 (100)	9 (69.2)	0.004
Ill defined	0 (0)	4 (30.8)	
Cystic changes			
Present	21 (61.8)	7 (59.6)	0.008
Absent	13 (38.2)	6 (40.4)	0.108
Infiltration to adjacent structures			
Present	0 (0)	4 (30.8)	0.004
Absent	34 (100)	9 (69.2)	
Perineural spread	0	2	
T1WI			
Hypointense	16 (47.1%)	3 (23.1)	0.004
Isointense	16 (47.1%)	8 (61.5)	0.152
Hyperintense	2 (5.8%)	2 (15.4)	1.0
T2WI			
Isointense	0 (0)	2 (15.4)	-
Hyperintense	27 (79.4)	3 (23.1)	<0.001
Heterogeneous	6 (17.6)	7 (53.8)	0.782
Hyperintense cystic with septations	1 (2.9)	1 (7.7)	1.0
Enhancement			
Homogeneous	8 (23.5)	1 (7.7)	0.410
Heterogeneous	25 (73.5)	12 (92.3)	
No enhancement	1 (2.9)	0 (0)	
Diffusion restriction			
Present	6/34 (17.6%)	12 (92.3)	<0.001
Absent	28/34 (82.4%)	1 (7.7%)	
ADC value (mm ² /s), mean ± SD (range)	1.75 ± 0.549 × 10 ⁻³	1.03 ± 0.314 × 10 ⁻³	<0.001
DCE TI curve			
Type A	28 (82.3)	2 (15.4)	<0.001
Type B	3 (8.8)	2 (15.4)	
Type C	2 (5.8)	9 (69.2)	
Type D	1 (2.9)	0 (0)	

Abbreviations: ADC, apparent diffusion coefficient; DCE, dynamic contrast-enhanced; MRI, magnetic resonance imaging; T1WI, T1-weighted imaging; SD, standard deviation.

Quantitative assessment of Ktrans, Ve, Kep, IAUGC, CER, and MS obtained from DCE-MRI is given in ►Table 3. One case of WT was excluded from calculation as values could not be obtained due to the complete cystic nature of the tumor.

NWBTs are well-defined round to oval lesions not showing restriction on DWI with a high ADC value and had low TBF in ASL. On DCE-MRI, NWBTs were showing type A curve and had low Ktrans, Kep, IAUGC, MS, and high Ve (►Fig. 2). WTs are well-defined lesions with areas of T1 hyperintense cystic areas, showing diffusion restriction with low ADC, high perfusion on ASL, type B curve in DCE-MRI with high Ktrans,

Kep, IAUGC, MS, and low Ve (►Fig. 3). MTs are heterogeneous lesions with a lobulated or infiltrative margin, show diffusion restriction on DWI, mostly showing type C TIC curve, high Ktrans, Kep, IAUGC, MS, and lower Ve (►Fig. 4). ►Tables 2 and 3 and the bar diagram in ►Fig. 5 show the mean values of all six parameters assessed for NWBTs, WTs, and MTs.

We found a similar result considering only pleomorphic adenoma in the NWBT group (without including other benign tumors). There was a significant difference between the mean ADC, TBF, and DCE parameters among pleomorphic adenomas, WTs, and MTs with a p-value less than 0.05. The mean ADC

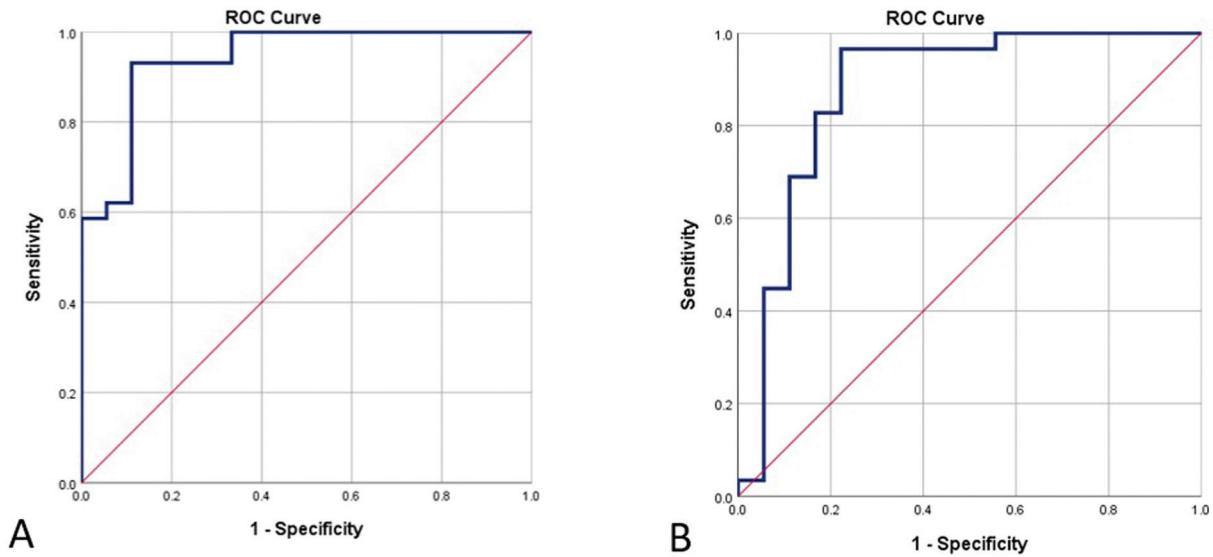


Fig. 1 Receiver operating characteristic (ROC) curve of (A) apparent diffusion coefficient (ADC) and (B) tumor blood flow (TBF) for diagnosis of non-Warthin's benign tumors. ADC from diffusion-weighted imaging is showing sensitivity of 93.1% and specificity of 88.9% (area under the curve [AUC]: 0.941) and TBF from arterial spin labeling showing sensitivity of 96.6% and specificity of 77.8% (AUC: 0.880).

Table 3 Comparison of the means ADC (from DWI), TBF (from pCASL), and DCE-MRI parameters among non-Warthin's benign tumors, Warthin's tumors, and malignant tumors

Sequences	Parameters	Non-Warthin's benign tumor vs. malignant tumors	Non-Warthin's benign tumor vs. Warthin's tumor	Malignant tumors vs. Warthin's tumor
DWI	ADC value ($\times 10^{-3}$ mm ² /s)	1.89 \pm 0.43 vs. 1.03 \pm 0.31 ($p < 0.001$)	1.89 \pm 0.43 vs. 0.97 \pm 0.45 ($p < 0.001$)	1.03 \pm 0.31 vs. 0.97 \pm 0.45 ($p = 0.96$)
ASL	TBF (mL/100 g/min)	21.99 \pm 12.62 vs. 70.33 \pm 36.18 ($p < 0.001$)	21.99 \pm 12.62 vs. 62.04 \pm 37.72 ($p = 0.015$)	70.33 \pm 36.18 vs. 62.04 \pm 37.72 ($p = 0.767$)
DCE-MRI	Ktrans (/min), mean \pm SD	0.191 \pm 0.13 vs. 0.45 \pm 0.31 ($p = 0.001$)	0.191 \pm 0.13 vs. 0.836 \pm 0.47 ($p = 0.001$)	0.453 \pm 0.31 vs. 0.836 \pm 0.47 ($p = 0.358$)
	Ve mean \pm SD	0.716 \pm 0.23 vs. 0.512 \pm 0.26 ($p = 0.011$)	0.716 \pm 0.23 vs. 0.407 \pm 0.10 ($p = 0.020$)	0.512 \pm 0.26 vs. 0.407 \pm 0.10 ($p = 0.489$)
	Kep (min ⁻¹), mean \pm SD	0.321 \pm 0.18 vs. 1.066 \pm 0.54 ($p = 0.001$)	0.321 \pm 0.18 vs. 2.39 \pm 1.71 ($p = 0.001$)	1.066 \pm 0.54 vs. 2.39 \pm 1.71 ($p = 0.46$)
	IAUGC, mean \pm SD	0.186 \pm 0.09 vs. 0.293 \pm 0.14 ($p = 0.014$)	0.186 \pm 0.09 vs. 0.472 \pm 0.27 ($p = 0.003$)	0.293 \pm 0.14 vs. 0.472 \pm 0.27 ($p = 0.185$)
	CER, mean \pm SD	1.69 \pm 0.70 vs. 1.37 \pm 0.54	1.69 \pm 0.70 vs. 1.74 \pm 0.56	1.37 \pm 0.54 vs. 1.74 \pm 0.56
	MS, mean \pm SD	0.0147 \pm 0.07 vs. 0.028 \pm 0.02 ($p = 0.001$)	0.0147 \pm 0.07 vs. 0.0529 \pm 0.04 ($p = 0.004$)	0.028 \pm 0.02 vs. 0.05 \pm 0.04 ($p = 0.439$)

Abbreviations: ADC, apparent diffusion coefficient; ASL, arterial spin labeling; CER, contrast enhancement ratio; DCE-MRI, dynamic contrast-enhanced magnetic resonance imaging; DWI, diffusion-weighted imaging; IAUGC, initial area under the gadolinium enhancement concentration curve; MS, maximum slope; pCASL, pseudo-continuous ASL; SD, standard deviation; TBF, tumor blood flow.

value of pleomorphic adenoma ($1.9 \pm 0.43 \times 10^{-3}$ mm²/s) was significantly higher than that of the WT ($0.97 \pm 0.45 \times 10^{-3}$ mm²/s; $p = .001$) and MT ($1.03 \pm 0.31 \times 10^{-3}$ mm²/s; $p = 0.001$). The mean TBF of the pleomorphic adenoma (21.9 ± 12.62 mL/100 g/min) was significantly less than that of WT (62.04 ± 37.72 mL/100 g/min; $p = 0.015$) and MT (70.33 ± 36.18 mL/100 g/min; $p < 0.001$). It could be due to the majority of benign cases in our series being pleomorphic adenomas.

Discussion

Our study included 47 patients of parotid gland tumor with a slight male predominance. Although the mean age of the patients with benign tumors was relatively less than that of the patient with MTs, it was not statistically significant.

In the morphological features, although there was considerable overlap between benign tumors and MTs, a round/oval or lobulated shape had a significant association

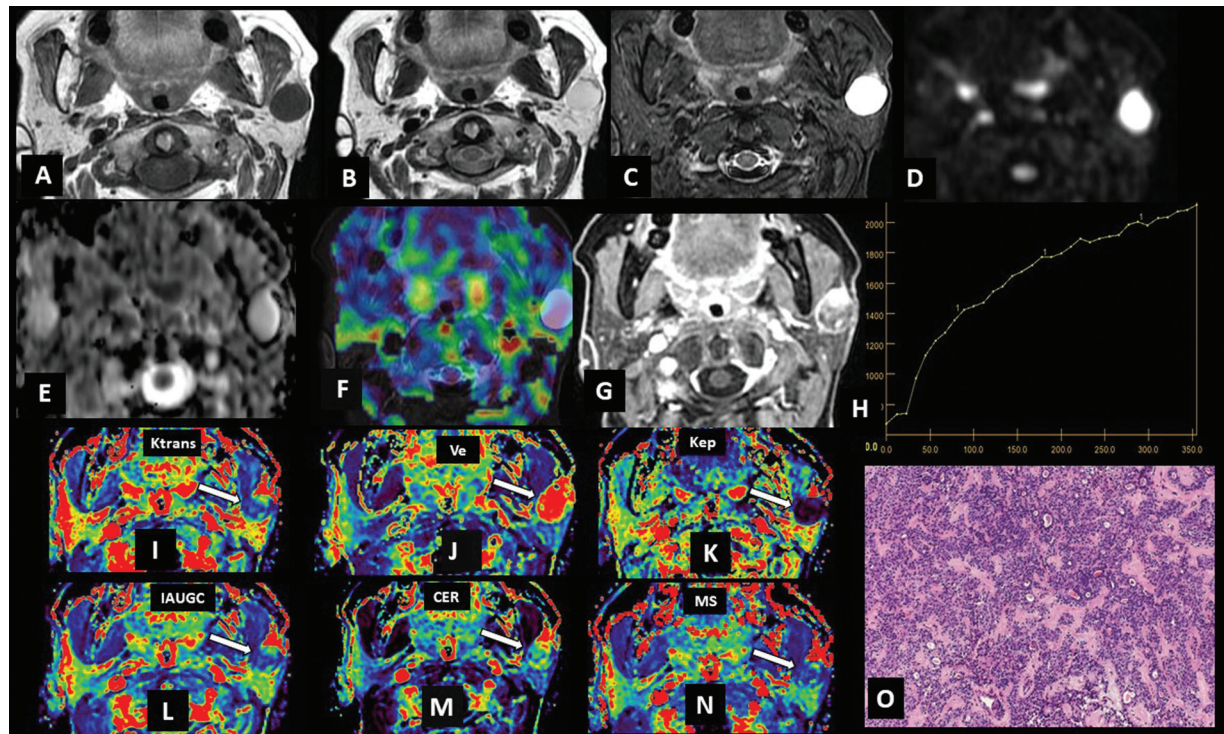


Fig. 2 Magnetic resonance imaging (MRI) of a 62-year-old woman having pleomorphic adenoma of the left parotid gland. Axial (A) T1-weighted imaging (T1WI), (B) T2WI, and (C) short tau inversion recovery (STIR) images show a well-defined rounded lesion involving the superficial lobe of the left parotid gland, which is hypointense on T1 and hyperintense on T2 and STIR. The lesion is hyperintense on both (D) diffusion-weighted imaging and (E) apparent diffusion coefficient, suggesting facilitated diffusion. (F) Arterial spin labeling shows reduced perfusion. (G) Postcontrast T1WI shows heterogeneous enhancement. (H) On dynamic contrast-enhanced MRI (DCE-MRI), type A time-intensity curve seen. Quantitative DCE shows (I) low K_{trans} (0.165/min), (J) high V_e (0.89), (K) low K_{ep} (0.187/min), (L) low IAUGC (0.192), (M) CER (2.224), and (N) low MS (0.0195), (O) histopathological examination showed epithelioid, myoepithelial, and stromal components suggestive of pleomorphic adenoma. CER, contrast enhancement ratio; IAUGC, initial area under the gadolinium enhancement concentration curve; MS, maximum slope.

with benign tumors, whereas infiltration into adjacent structures and ill-defined margins had a significant association with MTs similar to other studies.⁶ Hypointense signal on T1WI, hyperintense signal on T2WI, and the presence of internal cystic changes favored benign tumors. We could not find a significant difference in the type of enhancement between benign tumors and MTs.

DWI is increasingly being evaluated in the imaging of parotid gland tumors in recent years. DWI measures the Brownian movement of the water proton. Increased cellularity within the tumor restricts the movement and is seen as diffusion restriction on DWI with a low ADC value. Hence, MTs show diffusion restriction in general.^{7,8} However, it was found that although WTs are benign, they have a higher cellularity and hence may show restricted diffusion. We found a significantly low mean ADC value in MTs, and WTs compared with NWBTs. This may be attributed to the higher cellularity of the MTs, and WTs compared with NWBTs.

Among the NWBTs ($n=29$), two showed mild diffusion restriction and turned out to be pleomorphic adenomas on histopathology. Pleomorphic adenomas usually do not show diffusion restriction and have a higher ADC value (1.4×10^{-3} to 1.57×10^{-3} mm^2/s in various studies).^{9,10} However, some of the pleomorphic adenomas may show lower ADC values when there is a larger cellular component relative to the stromal component.¹¹ All of our cases of WT showed signifi-

cant diffusion restriction, except one, which was completely cystic without any solid component. We found an ADC cutoff of 1.35×10^{-3} mm^2/s differentiates NWBTs from MTs with sensitivity and specificity of 93.1 and 88.9%, respectively. An ADC cutoff of 1.446×10^{-3} mm^2/s can differentiate pleomorphic adenomas (the most common NWBT) from MTs with a sensitivity, specificity, and accuracy of 92.3, 81, and 87.2%, respectively. Studies have also shown a significant difference between the mean ADC value of WTs and MTs.¹² However, it was not statistically significant in our study. It could be due to a smaller number of WTs in our sample.

The ASL technique is a completely noninvasive method, typically accomplished by magnetically tagging the entering blood by spin inversion of arterial water using radiofrequency (RF) energy, without any exogenous contrast administration. Pseudo-continuous ASL (pCASL) uses multiple short RF pulses ($>1,000$) and has a lower effect of magnetization transfer, lower specific absorption rate, and a high signal-to-noise ratio (SNR). Further, 3-T MRI scanner improves the SNR of ASL.^{13,14} We found a significantly higher mean TBF in WTs than that of pleomorphic adenomas, similar to other studies.⁹

The role of DCE-MRI in parotid gland tumors has been a topic of interest in recent times. When an intravenous contrast agent is administered, it enters the circulatory system, passes through the neoplastic tissues, and leaks

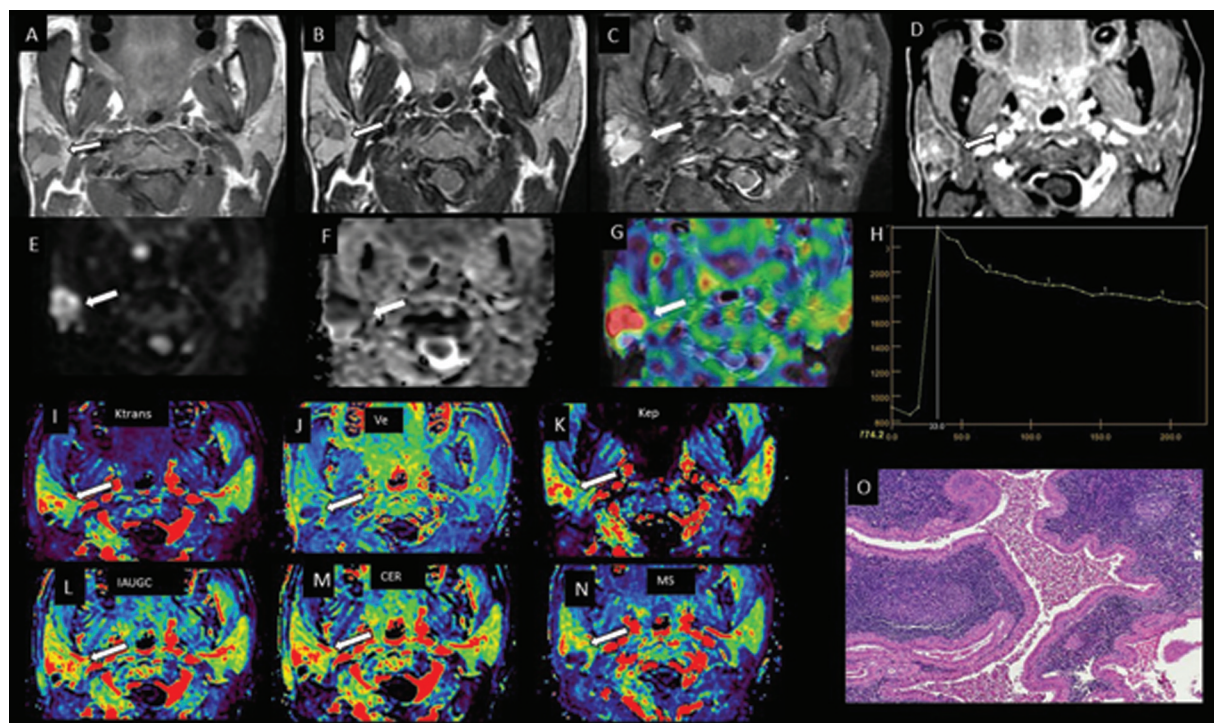


Fig. 3 Magnetic resonance imaging (MRI) of the parotid gland in a 31-year-old woman with Warthin's tumor (WT) of the right parotid gland. Axial (A) T1-weighted imaging (T1WI), (B) T2WI, and (C) short tau inversion recovery (STIR) images show a well-defined lobulated lesion with T1 hyperintense cystic areas, and heterogeneous signal on T2 and STIR. (D) Postcontrast T1WI shows heterogeneous enhancement. (E) Diffusion-weighted imaging and (F) apparent diffusion coefficient show restricted diffusion. (G) Arterial spin labeling shows increased perfusion. (H) On dynamic contrast-enhanced MRI (DCE-MRI), type B time-intensity curve noted. Quantitative DCE show a (I) high Ktrans (1.068/min), (J) low Ve (0.25), (K) high Kep (4.387/min), (L) high IAUGC (0.427), (M) CER (1.714), and (N) high MS (0.0515), (O) HPE display glandular architecture with extensive lymphoid stroma surrounding cystic regions with papillary projections bordered by oncocytes suggestive of WT. CER, contrast enhancement ratio; IAUGC, initial area under the gadolinium enhancement concentration curve; MS, maximum slope.

from the tumor vasculature into the EES by passive diffusion. Backflow of the contrast agent from the EES to plasma occurs as the contrast concentration in plasma gets reduced as a result of renal excretion. The intravascular space, the EES, and the intracellular space are the three compartments that make up all tissues, including cancerous tissue. The intravascular space and the EES are the only considered anatomic characteristics that affect contrast agent distribution for most of the DCE-MRI modeling.¹⁵⁻¹⁷ Qualitative parameters such as the TIC and quantitative parameters like Ktrans, Ve, Kep, IAUGC, CER, and MS can be evaluated using DCE-MRI. The time-to-peak intensity and WR, which reflect tumor vascularity and tumor cellularity, respectively, are used to classify the TICs into four patterns: types A to D.¹⁸

The pattern of TIC was highly sensitive to differentiate the subgroups of parotid gland tumors. Type A curve shows a high sensitivity and specificity for benign tumors (96.5 and 88.8%, respectively), and type C is more indicative of MTs. In this study, 96% of NWBTs showed a type A curve and most of the solid WTs showed a type B curve. One completely cystic WT showed a flat type D curve. Most of the MTs showed a type C curve, achieving a sensitivity of 69.2%, specificity of 94.1%, and accuracy of 87.2%. We found a relatively lower sensitivity as few of the MTs in this study also had a type B TIC. The sensitivity was 84.6% when both type B and C curves were considered as malignant. A study by

Mogen et al on the role of qualitative and semiquantitative DCE in parotid gland tumors showed a high sensitivity, specificity, PPV, and NPV for type A curve for identifying pleomorphic adenomas.¹⁹

Ktrans, known as the transfer factor, is a measure of the rate at which the contrast enters the EES from the intravascular space and, hence, is a measure of the permeability of the capillary vessels in the tumor. Ve is the fraction of EES to the total tumor volume. The ratio between Ktrans and Ve is called the flux constant (Kep). Ktrans and Kep reflect the microvascular permeability and are increased in MTs where there is more neoangiogenesis, with abnormal vessels having increased permeability. IAUGC, CER, and MS are the DCE parameters acquired in the initial 60 seconds after administration of contrast.

Studies have shown that MTs and highly cellular tumors like WTs show a higher Ktrans and Kep values and a lower Ve value.²⁰ There is paucity of studies about the role of parameters such as IAUGC, CER, and MS in differentiating parotid gland tumors. The mean Ktrans and Kep values were the highest in WTs and the least in NWBTs. The mean Ve was lowest in WTs and highest in NWBTs. This may be attributed to the lower perfusion and capillary permeability, lower cellularity, and higher extracellular extravascular volume in NWBTs and higher perfusion and cellularity in WTs. MTs also showed higher mean Ktrans and Kep values and lower Ve

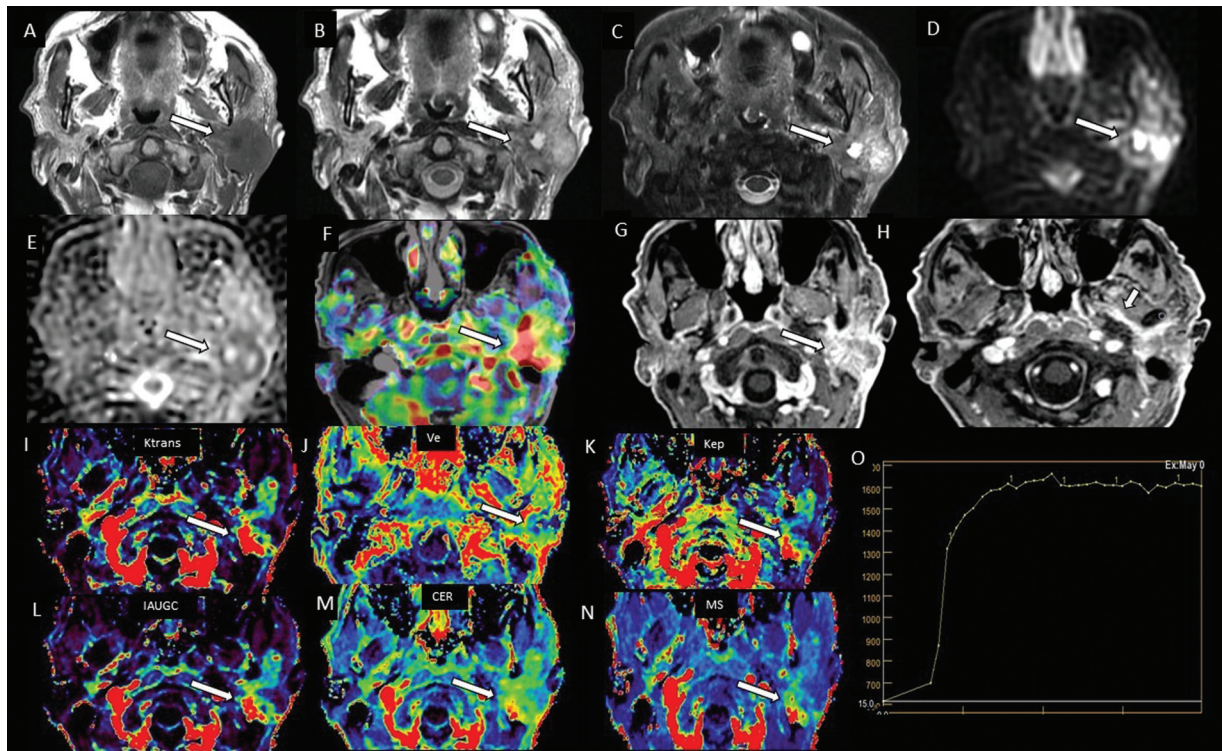


Fig. 4 Magnetic resonance imaging (MRI) of the parotid gland in a 64-year-old man with acinic cell carcinoma of the left parotid gland. Axial (A) T1-weighted imaging (T1WI), (B) T2WI, and (C) short tau inversion recovery images show an irregular lobulated lesion with heterogeneous signal and areas of cystic change. (D) Diffusion-weighted imaging and (E) apparent diffusion coefficient show restricted diffusion. (F) Arterial spin labeling shows increased perfusion. (G, H) Postcontrast T1WI shows heterogeneous enhancement and perineural spread along the mandibular division of left trigeminal nerve. (I) Quantitative dynamic contrast-enhanced (DCE) shows a high Ktrans (0.634/min), (J) low Ve (0.54), (K) high Kep (1.23/min), (L) high IAUGC (0.554), (M) CER (1.845), and (N) high MS (0.0834). (O) On DCE-MRI, type C time-intensity curve is seen. CER, contrast enhancement ratio; IAUGC, initial area under the gadolinium enhancement concentration curve; MS, maximum slope.

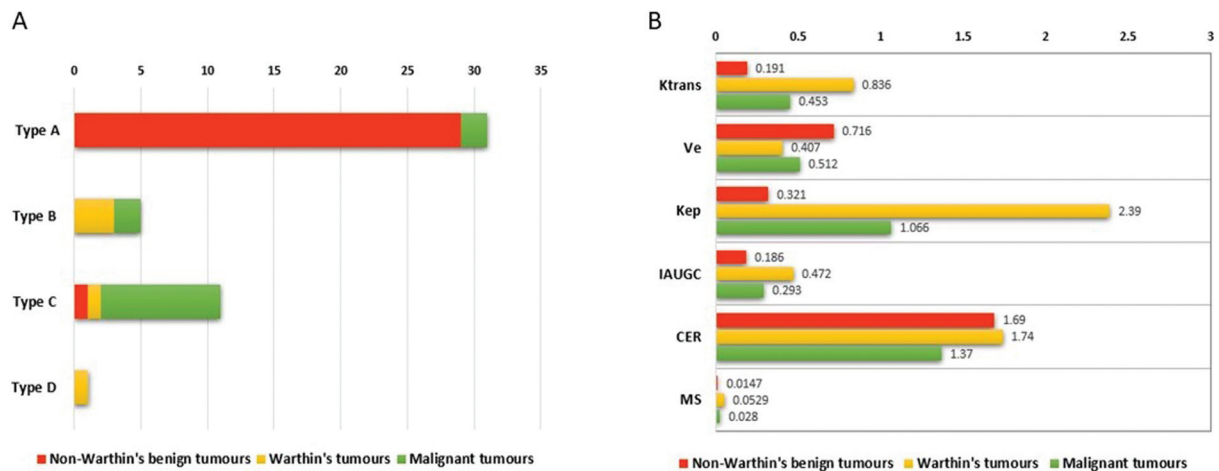


Fig. 5 Bar diagram showing (A) type of the time signal intensity curve and (B) quantitative dynamic contrast-enhanced (DCE) parameters in non-Warthin's benign tumor, Warthin's tumor, and malignant tumor of the parotid gland. CER, contrast enhancement ratio; IAUGC, initial area under the gadolinium enhancement concentration curve; MS, maximum slope.

compared with NWBTs owing to the same fact. We also found a significant difference in the IAUGC and MS among the various categories of tumors, whereas CER did not show any significant difference. The mean IAUGC and MS values were the least in NWBTs and the highest in WTs.

DCE-MRI reflects the microscopic composition of the tumor providing information about the microvasculature,

capillary permeability, and cellularity. Thus, it may act as a noninvasive technique to indirectly evaluate the tumor grade.

Both lymphomas and WTs show many similarities in functional sequences. Both show diffusion restriction with a low ADC value on DWI and high TBF in ASL sequences. On DCE-MRI, lymphoma can show type B signal intensity curve

as commonly seen in WTs. Structural sequences are very useful in these cases. Cystic degeneration with T1 hyperintense areas is commonly seen in WTs. Lymphomas are solid lesions with a homogeneous T1 and T2 signal and homogeneous postcontrast enhancement. Parotid gland lymphoma is commonly associated with cervical lymphadenopathy.

Considering the above-mentioned facts, multiparametric MRI with the addition of advanced functional MRI sequences like DWI, ASL, and DCE-MRI to the conventional MRI can aid in the diagnosis and evaluation of parotid gland tumors. By evaluating the time-intensity curves and the quantitative DCE parameters along with ADC and TBF values, it may also be possible to differentiate pleomorphic adenomas and WTs from other parotid tumors with a higher sensitivity, specificity, and accuracy.

The strengths of our study are the inclusion of multiple age groups and types of tumors, with a fairly representative sample size. The limitations of our study include an asymmetric distribution of the cases among NWBTs, WTs, and MTs. A larger sample size with a greater number of different subgroups may provide further insight into the current study. Further multicentric studies with a large sample with different histopathological subtypes will improve the results.

Conclusion

DWI can diagnose pleomorphic adenoma and NWBTs with high sensitivity, specificity, and accuracy. Although WT is benign, it shows a low ADC value due to its high cellular nature. DCE-MRI is the most sensitive functional MRI in the differentiation of the three major subgroups of parotid gland tumors. Multiparametric MRI using DWI, ASL, and DCE is useful in differentiating the major subgroups of parotid tumors.

Patient Consent

Written informed consent was obtained from all the patients included in the study.

Funding

None.

Conflict of Interest

None declared.

References

- 1 Stenner M, Klusmann JP. Current update on established and novel biomarkers in salivary gland carcinoma pathology and the molecular pathways involved. *Eur Arch Otorhinolaryngol* 2009; 266(03):333–341
- 2 Mallon DH, Kostalas M, MacPherson FJ, et al. The diagnostic value of fine needle aspiration in parotid lumps. *Ann R Coll Surg Engl* 2013;95(04):258–262
- 3 Perkins C, Toll E, Reece P. Fine-needle aspiration cytology and radiological imaging in parotid gland tumours: our experience in 103 patients. *Clin Otolaryngol* 2019;44(06):1124–1127
- 4 Yabuuchi H, Fukuya T, Tajima T, Hachitanda Y, Tomita K, Koga M. Salivary gland tumors: diagnostic value of gadolinium-enhanced dynamic MR imaging with histopathologic correlation. *Radiology* 2003;226(02):345–354
- 5 Coudert H, Mirafzal S, Dissard A, Boyer L, Montoriol PF. Multiparametric magnetic resonance imaging of parotid tumors: a systematic review. *Diagn Interv Imaging* 2021;102(03):121–130
- 6 Kushwaha M, Kumar J, Garg A, Singh I, Khurana N. Differentiation of various salivary gland tumours using diffusion-weighted MRI and dynamic contrast-enhanced MRI. *Pol J Radiol* 2023;88(88):e203–e215
- 7 Baliyan V, Das CJ, Sharma R, Gupta AK. Diffusion weighted imaging: technique and applications. *World J Radiol* 2016;8(09):785–798
- 8 Charles-Edwards EM, deSouza NM. Diffusion-weighted magnetic resonance imaging and its application to cancer. *Cancer Imaging* 2006;6(01):135–143
- 9 Razek AAKA. Multi-parametric MR imaging using pseudo-continuous arterial-spin labeling and diffusion-weighted MR imaging in differentiating subtypes of parotid tumors. *Magn Reson Imaging* 2019;63:55–59
- 10 Yabuuchi H, Matsuo Y, Kamitani T, et al. Parotid gland tumors: can addition of diffusion-weighted MR imaging to dynamic contrast-enhanced MR imaging improve diagnostic accuracy in characterization? *Radiology* 2008;249(03):909–916
- 11 Kato H, Kawaguchi M, Ando T, Mizuta K, Aoki M, Matsuo M. Pleomorphic adenoma of salivary glands: common and uncommon CT and MR imaging features. *Jpn J Radiol* 2018;36(08):463–471
- 12 Ikeda M, Motoori K, Hanazawa T, et al. Warthin tumor of the parotid gland: diagnostic value of MR imaging with histopathologic correlation. *AJNR Am J Neuroradiol* 2004;25(07):1256–1262
- 13 Iutaka T, de Freitas MB, Omar SS, et al. Arterial spin labeling: techniques, clinical applications, and interpretation. *RadioGraphics* 2023;43(01):e220088
- 14 Domi T, Vossough A, Stence NV, et al. The potential for advanced magnetic resonance neuroimaging techniques in pediatric stroke research. *Pediatr Neurol* 2017;69:24–36
- 15 Knopp MV, Weiss E, Sinn HP, et al. Pathophysiologic basis of contrast enhancement in breast tumors. *J Magn Reson Imaging* 1999;10(03):260–266
- 16 Paldino MJ, Barboriak DP. Fundamentals of quantitative dynamic contrast-enhanced MR imaging. *Magn Reson Imaging Clin N Am* 2009;17(02):277–289
- 17 Gordon Y, Partovi S, Müller-Eschner M, et al. Dynamic contrast-enhanced magnetic resonance imaging: fundamentals and application to the evaluation of the peripheral perfusion. *Cardiovasc Diagn Ther* 2014;4(02):147–164
- 18 Abdel Razek AAK, Mukherji SK. State-of-the-art imaging of salivary gland tumors. *Neuroimaging Clin N Am* 2018;28(02):303–317
- 19 Mogen JL, Block KT, Bansal NK, et al. Dynamic contrast-enhanced MRI to differentiate parotid neoplasms using golden-angle radial sparse parallel imaging. *AJNR Am J Neuroradiol* 2019;40(06):1029–1036
- 20 Gökçe E, Beyhan M. Advanced magnetic resonance imaging findings in salivary gland tumors. *World J Radiol* 2022;14(08):256–271